

Differential Scanning Calorimetry (DSC) and Thermodynamic Prediction of Liquid Fraction vs Temperature for Two High-Performance Alloys for Semi-Solid Processing (Al-Si-Cu-Mg (319s) and Al-Cu-Ag (201))



DUYAO ZHANG, HELEN V. ATKINSON, HONGBIAO DONG, and QIANG ZHU

There is a need to extend the application of semi-solid processing (SSP) to higher performance alloys such as 319s (Al-Si-Cu-Mg) and 201 (Al-Cu-Ag). The melting of these two alloys was investigated using differential scanning calorimetry (DSC) and thermodynamic prediction. The alloys had been processed by magneto-hydrodynamic (MHD) stirring before receipt to produce a microstructure suitable for SSP. The DSC results for the as-received MHD material were compared with those for material which has been taken through a complete DSC cycle and then reheated for a second DSC run. The effects of microsegregation were then analyzed. A higher liquid fraction for a particular temperature is found in the second DSC run than the first. Microstructural observations suggest this is because the intermetallics which form during the first cooling cycle tend to co-located. Quaternary and ternary reactions then occur during the second DSC heat and the co-location leads to enhanced peaks. The calculated liquid fraction is lower with 10 K/min DSC heating rate comparing with 3 K/min at a given temperature. The DSC scan rate must therefore be carefully considered if it is to be used to identify temperature parameters or the suitability of alloys for SSP. In addition, the starting material for DSC must represent the starting material for the SSP. With thermodynamic prediction, the equilibrium condition will provide better guidance for the thixoforming of MHD stirred starting material than the Scheil condition. The Scheil mode approximates more closely with a strongly microsegregated state.

DOI: 10.1007/s11661-017-4235-2

© The Author(s) 2017. This article is an open access publication

I. INTRODUCTION

SEMI-SOLID metal (SSM) processing is a powerful technology (with several variants including thixoforming and rheocasting) for forming alloys in the semi-solid state to near net-shaped products (*e.g.*, Reference 1). For thixoforming (which involves reheating billet

material from the solid state into the semisolid state), the liquid fraction for processing is typically between 30 vol pct and 50 vol pct. The process relies on the presence of a microstructure consisting of spheroids (globules) of solid in a liquid matrix when the material is in the semisolid state. With conventionally cast aluminum alloys such as A356 and A357, excellent mechanical properties can be achieved by SSM in comparison with the conventional casting routes. There are more challenges with high strength aluminum alloys (such as the silver-containing 201, or the Al-Si hypoeutectic Cu-containing alloy 319) often due to hot cracking during the final stages of forming. These alloys usually contain copper, a key alloying element which contributes to the strength and age hardening response, but can also increase hot tearing.^[2] The excellent castability and good mechanical properties of 319 Al alloy (Al-6Si-3.5Cu-0.1 Mg wt pct) and 201 alloy (Al-5Cu-0.35Mg-0.35Mn-0.7Ag) give them widespread application in the automotive and aerospace industry, respectively.^[3,4] Alloy 319s is a primary version of the low-cost foundry alloy 319 to enhance the suitability for

DUYAO ZHANG is with the School of Engineering, RMIT University, 115 Queensberry St, Melbourne, VIC, 3053, Australia. HELEN V. ATKINSON is with the Department of Engineering, University of Leicester, University Rd., Leicester, LE1 7RH, UK, and also with the School of Aerospace, Transport and Manufacturing, Cranfield University, College Rd., Bedford, MK43 0AL, UK. Contact e-mails: hva2@le.ac.uk, Helen.Atkinson@cranfield.ac.uk HONGBIAO DONG is with the Department of Engineering, University of Leicester. QIANG ZHU is with the Department of Mechanical and Energy Engineering, Southern University of Science and Technology, No 1088, Xueyuan Rd., Shenzhen, Guangdong, 518055, China.

Manuscript submitted on March 2, 2017.

Article published online July 31, 2017

Table I. Solidification Reactions in 319 Alloy from Bäckerud *et al.*^[3]

Reaction	Suggested Temperature [K (°C)]
1. Liq. → α -Al	882 K (609 °C)
2a. Liq. → Al + Al ₁₅ (FeMn) ₃ Si ₂	863 K (590 °C)
2b. Liq. → Al + Si + Al ₅ FeSi	863 K (590 °C)
3. Liq. → Al + Si + Al ₅ FeSi	848 K (575 °C)
4. Liq. → Al + Al ₂ Cu + Si + Al ₅ FeSi	798 K (525 °C)
5. Liq. → Al + Al ₂ Cu + Si + Al ₅ Mg ₈ Cu ₂ Si ₆	780 K (507 °C)

Note that these are for alloy 319 with composition Al-5.7Si-3.4Cu-0.62Fe-0.1Mg-0.92Zn-0.14Ti-0.36Mn, wt pct) rather than 319s (see Table III).

Table II. Solidification Reactions in 319 Alloy from Samuel *et al.*^[4]

Reaction	Suggested Temperature [K (°C)]
1. (Al) Dendrite network	883 K (610 °C)
2. Precipitation of eutectic Si	835 K (562 °C)
3. Precipitation of Al ₆ Mg ₃ FeSi ₆ + Mg ₂ Si	827 K (554 °C)
4. Precipitation of Al ₂ Cu	783 K (510 °C)
5. Precipitation of Al ₅ Mg ₈ Cu ₂ Si ₆	763 K (490 °C)

Note that these are for alloy 319 (Al-5.95Si-3.56Cu-0.11Fe-0.5Mg-0.145Ti-0.01Ni-0.02Mn, wt pct) rather than 319s (see Table III).

thixoforming. The mechanical properties of semi-solid processed 319s in the T6 state are significantly higher than those for permanent mould cast 319-T6.^[3]

There is important literature^[5,6] on the solidification reactions for this alloy which will be identified below as part of developing the framework for this paper even though the semi-solid processing (SSP) route involves heating rather than cooling. 319 alloy has two main solidification reactions, the formation of Al dendrites followed by the development of the two-phase Al-Si eutectic. However, the Cu and Mg which are also present, as well as impurities such as Fe and Mn, lead to more complex solidification reactions and at room temperature the microstructure will contain many intermetallic phases. The solidification reactions have been reported by Bäckerud *et al.*^[5] and by Samuel *et al.*^[6] and are shown in Tables I and II, respectively.

The two solidification sequences differ between Tables I and II. After the crystallization of Al dendrites, the phases Al₁₅(FeMn)₃Si₂ together with Al₅FeSi identified by Bäckerud *et al.*^[5] were not reported by Samuel *et al.*^[6] probably because of the higher Mn and Fe contents in the Bäckerud *et al.*^[5] alloy. The Al-Si eutectic reaction temperature of 835 K (562 °C) for Samuel *et al.*^[6] is much lower than that of 848 K (575 °C) in Bäckerud *et al.*^[5] (Bäckerud *et al.*^[5] identify this as ternary reaction but in practice, given that the binary eutectic to form Si is likely to occur, the reaction

is probably a superposition of two closely occurring reactions which were difficult to separate with the experimental methods available). Samuel *et al.*^[6] suggested that this temperature was depressed by the increased Si content of the alloy (compare the alloy compositions in the Table captions). The precipitation of Al₆Mg₃FeSi₆ and Mg₂Si at 827 K (554 °C) was observed by Samuel *et al.*^[6] with relatively high Mg (0.5 wt pct) content. This reaction has also been detected by Martinez *et al.*^[7] with 0.3 wt pct Mg. The four-phase reaction at 798 K (525 °C) in Bäckerud *et al.* relates to the start of Al₂Cu precipitation. The Al₅FeSi in that reaction might be inherited from the reactions which have occurred at higher temperature. For both references, Al₅Mg₈Cu₂Si₆ precipitates out at a lower temperature than the start of the Al₂Cu precipitation.

A key parameter for SSM processing is the slope of the liquid fraction versus temperature curve between 30 pct liquid and 50 pct, which should be low to give a processing window.^[8–10] Below 30 pct liquid there tends not to be enough liquid present to enable the round globules to flow past each other and hence fill the die effectively and above 50 pct the billet is prone to collapse during handling. In addition, Liu *et al.*^[10] identified that the eutectic ‘knee’ can act as a kinetic ‘brake’ in heating the billet from solid *i.e.*, there is an arrest at the temperature of the eutectic reaction until the reaction is complete before further melting proceeds. They have identified that it is the coincidence between this eutectic knee and ~50 pct liquid which means that A356 alloy (Al ~7 pctSi) is eminently suitable for SSP (and hence widely used for this process commercially); if the knee occurred at a higher amount of liquid, the billet would have a much greater tendency to collapse before the liquid which should be present throughout the structure has fully developed. To identify the process parameters in advance of practical tests, the fraction liquid versus temperature curve is often obtained by Differential Scanning Calorimetry (DSC) even though the heating rate in DSC is typically 10 K/min, whereas that in induction heating of the billet in the thixoformer will be perhaps an order of magnitude higher (typically 75 K/min). A number of researchers have carried out DSC tests on 319 alloys in the literature or have discussed the use of DSC in obtaining solid fraction versus temperature in relation to SSP (*e.g.*, References 11–18). In addition, thermodynamic prediction (*e.g.*, *via* software packages such as Thermo-Calc) is increasingly used.^[10,19–21] There is, however, a lack of information evaluating the influence of microsegregation on liquid fraction prediction from DSC. This paper summarizes the influence of microsegregation on the DSC curves and the comparison with those from thermodynamic prediction.

II. EXPERIMENTAL PROCEDURES

Commercial 319s and 201 aluminum alloys were used in this study. Both alloys were produced by SAG in Austria using the MHD stirring process. The chemical compositions of the as-received alloys and the aluminum alloy (AA) standard compositions^[22] are given in Table III.

Table III. Chemical Compositions (Wt Pct) of the Alloys

Alloys	Chemical Compositions (Wt Pct)							
	Cu	Si	Mg	Ti	Mn	Fe	Zn	Ag
319s (actual)	2.95	6.10	0.37	0.05	0.02	0.12	0.02	—
319s (standard)	2.5-3.5	5.5-6.5	0.3-0.4	0.2	0.03	0.15	0.05	—
319 (AA standard)	3.0-4.0	5.5-6.5	<0.1	<0.25	<0.5	<0.8	<1.0	—
201 (actual)	4.80	0.09	0.25	0.25	0.29	0.15	—	0.70
201 (AA standard)	4.0-5.20	<0.1	0.15-0.55	0.15-0.35	0.15-0.50	<0.1	—	0.40-1.0

The 'actual' values were obtained by inductively coupled plasma atomic emission spectroscopy (ICP-AES) at SAG.

Differential scanning calorimetry analysis was performed on a NETZSCH 404 DSC in an argon-controlled environment. The high-purity Al_2O_3 pan was used as reference material. The mass of the specimen used for DSC analysis was around 20 mg, and the sample was cut from the center of the as-received alloys. The standard heating rate in the DSC is 3 K/min. The samples were heated to 993 K (720 °C) at 3 K/min, held for 5 min, and then cooled to 303 K (30 °C) at the same rate, followed by a second repetition of the same route (called 2nd heating). Argon was fed through the system at a flow rate of 35 ml/min to minimize oxidation of the samples. Three repetitions were carried out for each sample, and a high reproducibility is obtained. The baselines were obtained by empty sample crucible measurements. The evaluation of the liquid phase fraction is carried out by the application of peak partial area integration (e.g., Reference 23), determining the reaction temperature by examining the intersection of the baseline and the extrapolated tangent line of the heat flow peak (e.g., Reference 24). Experiments were also carried out with the 319s at a higher heating rate of 10 K/min.

For image analysis, the alloy in the as-received state and after cooling in the DSC was compared. All samples were final polished with 0.25 micron colloidal silica media without etching. Scanning Electron Microscopy (SEM Sirion 200) with energy dispersive X-ray analysis (EDX, Oxford INCA 350) was carried out to characterize microstructures.

Comparison between Scheil and equilibrium thermodynamic calculations was carried out using Thermo-Calc (Version: TCW5), with database TTAL7^[25] for the 319s alloy. The actual chemical composition of 319s alloy was used (as given in the first line of Table III). The equilibrium is based on the lever rule, while the Scheil model is applied with five basic assumptions (e.g., Reference 26):

- Equilibrium interface
- No back diffusion in the solid phase
- Homogenous compositions in liquid phase
- Equal densities of the solid and liquid phases
- No undercooling effect

Liu *et al.*^[10] have described the origins of error in such calculations.

The liquid fraction is a critical parameter both for fundamental work and for the control of SSM processing. Therefore, comparisons between thermodynamic

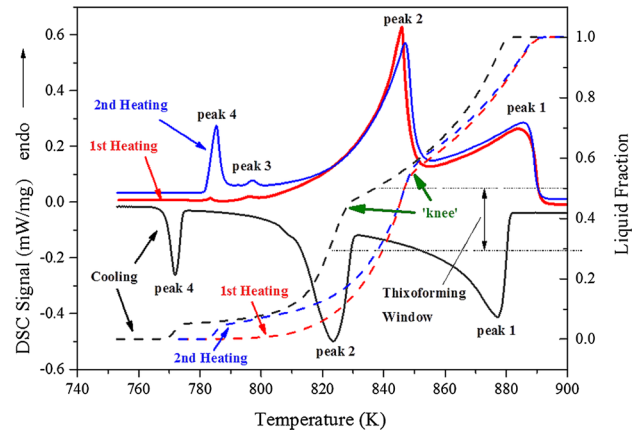


Fig. 1—Measured DSC signal vs temperature and calculated liquid fraction vs temperature for 319s alloy with rate 3 K/min. (The solid line is the DSC curve and the dashed line is liquid fraction).

calculations and DSC results for the 319s alloy are discussed here. It should be pointed out that the Ag element is not available in the Thermo-Calc database, so the thermodynamic prediction result for the 201 alloy could not be calculated.

III. RESULTS AND DISCUSSION

A. DSC Characterization

The results of DSC trace curves and calculated liquid fraction vs. temperature for 319s alloy are shown in Figure 1. The '2nd heating' means the sample was heated from 303 K (30 °C) to the fully liquid state and cooled in the '1st heating' and then, immediately on cooling to 303 K (30 °C), reheated through the same cycle. As the sample was completely melted and then the cooling controlled by the DSC at a constant rate (3 K/min in Figure 1), the cooling can be regarded as a slow solidification process. The melting curves show four temperature arrests (peak 4, peak 3, peak 2, peak 1) but there are only three for the cooling curve (labeled peak 1, peak 2, peak 4). Peaks 1, 2, and 4 are correspondent with the following reactions (Table IV) in Bäckerud *et al.*^[5]

There is some uncertainty about Peak 2 which in Table I occurs at 863 K (590 °C) but in the DSC cooling trace is occurring at about 829 K (556 °C). However, in this paper, the Mn content of alloy 319s is relatively low,

so reaction 2a in Table I is unlikely to occur. Peak 2 in Figure 1 is likely to identify with Reaction 3 in Table I. Peak 3 was not reported in previous literature.

The parameters calculated from melting and cooling curves in Figure 1 are summarized in Table V. Undercooling occurs during solidification, so the start and finish temperatures for the peaks tend to be lower during cooling than during the heating cycle. It is suggested in the literature^[12,27] that during heating the Al₂Cu phase may undergo gradual dissolution in the α -Al matrix until the reaction temperature for the Al₂Cu phase is reached at 783 K (510 °C). It is clear that peak 4 increases in height on the 2nd heating curve, comparing with the 1st heating curve, and is shifted slightly to the higher temperatures. This is also the case for Peak 3. For Peak 2, however, the peak for 1st heating is at a slightly higher temperature than that for 2nd heating.

The disappearance of peak 3 can also be seen on the cooling curve in Figure 1. If peak 3 is the quaternary reaction to form Al₅Mg₈Cu₂Si₆, this suggests this phase has fully dissolved on heating to the liquid state and then has not precipitated out to a detectable extent on cooling. In the '2nd heating' cycle, it reappears as a just detectable peak.

Considering the calculated liquid fraction versus temperature, the 'knee' (arrows in Figure 1) for the heating is associated with ~9 pct more liquid fraction and ~20 K (-253 °C) higher temperature than for the cooling curve. However, inspection of the thixoforming window shows that by the time the temperature has been reached at which ~30 pct liquid would be expected to be present, the 1st heating and 2nd heating curves have converged, and the temperature window would be almost identical. The distinction in fraction liquid versus temperature for the two heats is below this regime.

The results in Figure 1 are for a DSC heating rate of 3 K/min. They are compared with a heating rate of 10 K/min in Figure 2. Figure 2(b) focusses on the

beginning of the melting process (*i.e.*, around the position of Peak 4). A higher heating rate for the DSC mimics the real thixoforming processing route more closely (although the DSC cannot achieve the actual heating rate which occurs in the billet), but the heating rate for the DSC should be chosen carefully, including because, in general, a higher heating rate may lead to the peaks overlapping.^[28] With a higher heating rate, generally peaks will tend to be moved to the higher temperature. Figure 2 shows that Peak 4 is moved slightly to the higher temperature but also tends to be enhanced with the higher heating rate. In contrast, Peak 3 appears to be slightly shifted to the left and to be hardly enhanced at all, suggesting that there has been some influence on the Peak 3 reaction from the Peak 4 reaction. The calculated liquid fraction in Figure 2 in the region of Peak 4 indicates that an additional 0.4 pct of liquid phase was forming with the higher heating rate. However, Figure 2(a) shows that in general, the higher heating rate gives a lower liquid fraction for a particular temperature. The DSC signal peaks for 10 K/min are higher than those for 3 K/min. This was checked by scrutinising the original data and integrating the heat flow (DSC signal) against time to obtain the enthalpy change over temperature. The enthalpies are similar, and therefore the difference between the traces is due to the inverse proportional relationship between time and heating rate, *i.e.*, for the higher heating rate, there is less time to form liquid. Inspecting the thixoforming widow of ~30 pct fraction liquid to ~50 pct, if the 3 K/min curve were used to indicate a thixoforming temperature the curve would suggest that ~860 K (587 °C) was the maximum temperature before the liquid fraction of 50 pct was exceeded but this would be the temperature at which, using the 10 K/min curve, the billet had only just achieved 30 pct liquid.

Figure 3 shows the DSC trace curves and calculated liquid fraction vs temperature for 201 alloy, and the temperatures for the reactions are summarized in Table VI. The peaks 1', 2', and 3' are correspondent with the following reactions according to Bäckerud *et al.*^[5] (which, note again, deals with solidification rather than melting), respectively. Peak 3' is stronger on 2nd heating than on 1st heating and slightly shifted to the higher temperature, indicating a similar behavior to Peak 4 with 319s alloy. In both cases, a quaternary reaction is involved. With the 2nd heat, about 5pct more

Table IV. Possible Identity of Peaks in Fig. 1 Based on Reactions in Table I

Peak: Reaction
1. Liq. → α -Al
2. Liq. → Al + Si + Al ₃ FeSi
4. Liq. → Al + Al ₂ Cu + Si + Al ₅ Mg ₈ Cu ₂ Si ₆

Table V. Temperatures (K) for Reaction Peaks Calculated From DSC Melting and Cooling Curves for 319s Alloy

Reaction Peak	Reaction Start	Reaction End	Reaction Range	Solidification Start	Solidification End	Solidification Range
1	848.9 K (575.7 °C)	890.5 K (617.3 °C)	41.6	882.4 K (609.2 °C)	828.9 K (555.7 °C)	53.5
2	829.6 K (556.4 °C)	848.9 K (575.7 °C)	19.3	828.9 K (555.7 °C)	810.3 K (537.1 °C)	18.6
3	794.9 K (521.7 °C)	799.8 K (526.6 °C)	4.9	—	—	—
4	783.4 K (510.2 °C)	788.7 K (515.5 °C, 1st heating) 785.0 K (511.8 °C, 2nd heating)	5.3 (1st heating) 1.6 (2nd heating)	774.6 K (501.4 °C)	769.3 K (496.1 °C)	5.3

Peaks 1, 2, and 3 are the same for both 1st and 2nd heating, but Peak 4 does differ and so both 1st and 2nd heating for Peak 4 are identified in the Table above.

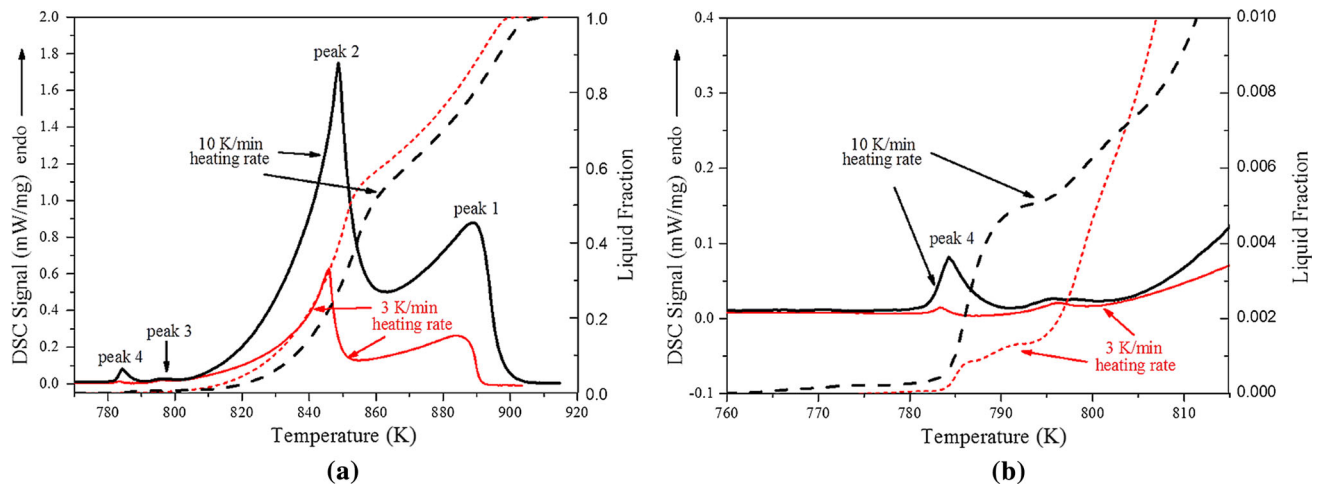


Fig. 2—Measured DSC signal range vs temperature and calculated liquid fraction vs temperature for 319s alloy with heating rate 3 K/min and 10 K/min (a) whole melting range (b) focussing on the beginning of melting. Both curves are for ‘1st heating’. (The solid line is the DSC curve and the dashed line is liquid fraction).

liquid is formed in that initial peak (Peak 3’) than on the 1st heat. On the other hand, for the thixoforming window, the 1st and 2nd heat are just about identical for fraction liquid vs temperature, although on cooling, for a given temperature, solidification is delayed. Table VII shows the start and end temperatures for the various reaction peaks, both on heating and on cooling.

B. Microstructure

Microstructures for 319s alloy in the as-received MHD processed state and after the whole of the DSC test (both ‘1st heating’ and ‘2nd heating’) are shown in Figure 4. It can be seen that the fine and spheroidal MHD microstructure becomes a microstructure with coarse and large secondary phases after DSC slow cooling. In addition, there is some evidence of shrinkage porosity in the slow cooled microstructure (Figure 4(b)) and also the Al_2Cu phases (which appear ‘bright’ in back scattered SEM images) are not present throughout the field of view. The Al-Si and Al_2Cu phases are separated in Figure 4(b).

Microstructures and EDX analysis of an area rich in copper phases in the 319s alloy are shown in Figure 5. The identity of the intermetallics is indicated by the combination of EDX results, together with thermodynamic calculations (Thermo-Calc) and References 5, 6, and 12. Figures 5(a) and (b) shows the as-received structure, in which the aluminum matrix is globular. The silicon phases and copper phases are finely and evenly distributed in the grain boundaries between the aluminum globules. After the DSC test, *i.e.*, slow solidification, the microstructure is a typical cast microstructure, as shown in Figures 5(c) and (d). Comparing Figures 5(a) and (c), the main copper-based phase is much coarser and more block-like in the sample slow-cooled through the DSC experiment. The intermetallics are also co-located and this then influences the DSC curve on reheating as these co-located phases are

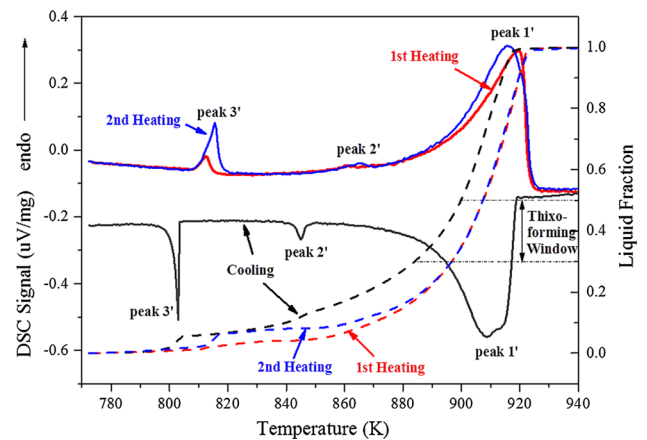


Fig. 3—Measured DSC signal vs temperature and calculated liquid fraction vs temperature for 201 alloy with rate 3 K/min. (The solid line is the DSC curve and the dashed line is liquid fraction).

giving rise to the quaternary and ternary reactions such as Peak 4 (Reaction 4) in Table IV and consequently the distinction between the DSC result on first heating and that on second heating.

A high-magnification micrograph, Figure 5(d), shows the details of the polynary phases in conjunction with Al_2Cu phase. The needle-shaped β phase (Al_3FeSi) and the $Al_5Mg_8Cu_2Si_6$ are formed along with the Al_2Cu phase. However, these polynary phases are barely distinguishable in the as-received microstructure. Considering the microstructures in relation to the DSC heating curves, there is good agreement with the changes of Peak 4 in Figure 1. Fine and evenly distributed Al_2Cu phase can be easily dissolved into the matrix in the as-received MHD processed alloy. The results of EDX quantitative line analysis across a grain and a grain boundary are given in Figures 5(g) and (h); the microsegregation is much enhanced after the slow solidification involved in the DSC experiment.

The microstructural results are fundamentally supporting a hypothesis that the distinction between the first heating and the second heating is due to the microsegregation which occurs during the solidification from the liquid state after the first heat.

The microstructure of 201 alloy after the DSC test shows the expected coarse copper phases and strong microsegregation (Figure 6). In Figures 6(d) and (e), the intermetallic compounds (likely to be $\text{Al}_{20}\text{Mn}_3\text{Cu}_2$ and Al_7FeCu_2) grow closely associated with Al_2Cu phase, which relates to the enhanced peak 3' on the 2nd heating curve (Figure 3) in comparison with the 1st heat. The acicular Al_7FeCu_2 phase in Figures 6(c) and (d) is clearly observed along with the Al_2Cu phase. The black and round $\text{Al}_{20}\text{Mn}_3\text{Cu}_2$ phases are surrounded by the secondary copper phases. These two intermetallic phases were identified by comparison with Reference 5 and in phase calculations (Thermo-Calc) with additional evidence from the EDX quantitative analysis in Figures 6(f) and (g). Two line analyses across the grain

boundaries are shown in Figures 6(i) and (j), respectively. The content of Cu increases in the region of the boundary due to the intermetallic phases associated with it. The average Cu content within the grain in the as-received is lower than for the slowly cooled 201 alloy, consistent with the concentration of the Cu in the phases at the boundary in the latter.

C. Thermodynamic Calculations for 319s Alloy

The predicted phases (assuming the Scheil condition) for 319s alloy using Thermo-Calc are shown in Figure 7, and the reaction temperatures for each phase are summarized in Table VIII. The reaction temperatures differ slightly from the experimental results partly because the precise composition of the alloy is different. Regarding the minor phases, these phases are only observed in the microstructure after the first DSC cycle (Figures 5(c) and (d)), and not in the as-received MHD processed sample (Figures 5(a) and (b)). This suggests

Table VI. Temperatures for Reactions in Alloy 201 Based on DSC Results in Fig. 3

Reaction	Suggested Temperature [K (°C)]
1'. Liq. \rightarrow α -Al	925 K (652°C)
Liq. \rightarrow Al + $\text{Al}_6(\text{MnFeCu})$	922 K (649°C)
2'. Liq. + $\text{Al}_6(\text{MnFeCu}) \rightarrow$ Al + $\text{Al}_{20}\text{Mn}_3\text{Cu}_2$	890 K (617°C)
3'. Liq. \rightarrow Al + Al_2Cu + $\text{Al}_{20}\text{Mn}_3\text{Cu}_2$ + Al_7FeCu_2	798 K (525°C)

Table VII. Temperatures (K) for Reaction Peaks Calculated from DSC Melting and Cooling Curves 201 Alloy

Reaction Peak	Reaction Start	Reaction End	Reaction Range	Solidification Start	Solidification End	Solidification Range
1'	889.7 K (616.5 °C)	925.8 K (652.6 °C)	36.1	918.6 K (645.4 °C)	890.8 K (617.6 °C)	27.8
2'	858.8 K (585.6 °C)	870.3 K (597.1 °C)	11.5	847.8 K (574.6 °C)	842.6 K (569.4 °C)	5.2
3'	809.2 K (536.0 °C, 1st heating)	815.4 K (542.2 °C, 1st heating)	6.2 K (1st heating)	803.8 K (530.6 °C)	800.6 K (527.4 °C)	3.2
	809.2 K (536.0 °C, 2nd heating)	818.2 K (545.0 °C, 2nd heating)	9.0 K (2nd heating)			

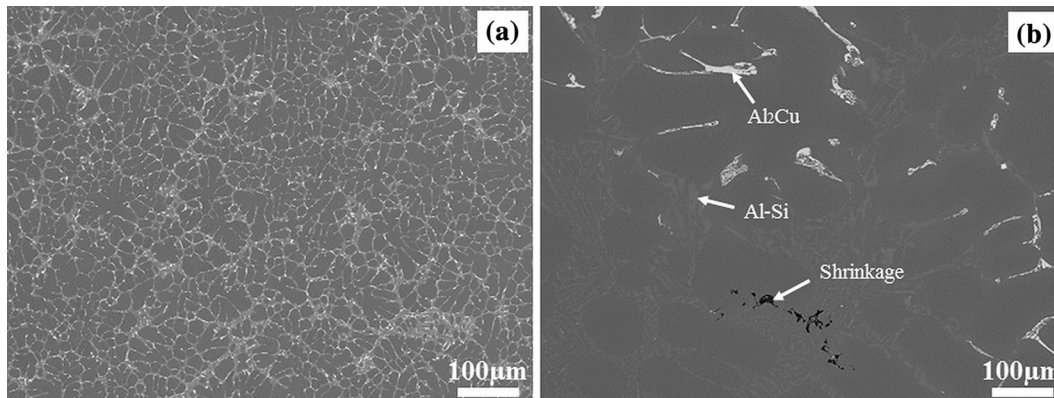


Fig. 4—SEM back scattered images of the 319s alloy: (a) as MHD processed, (b) after DSC test (3 K/min with ~20 mg sample).

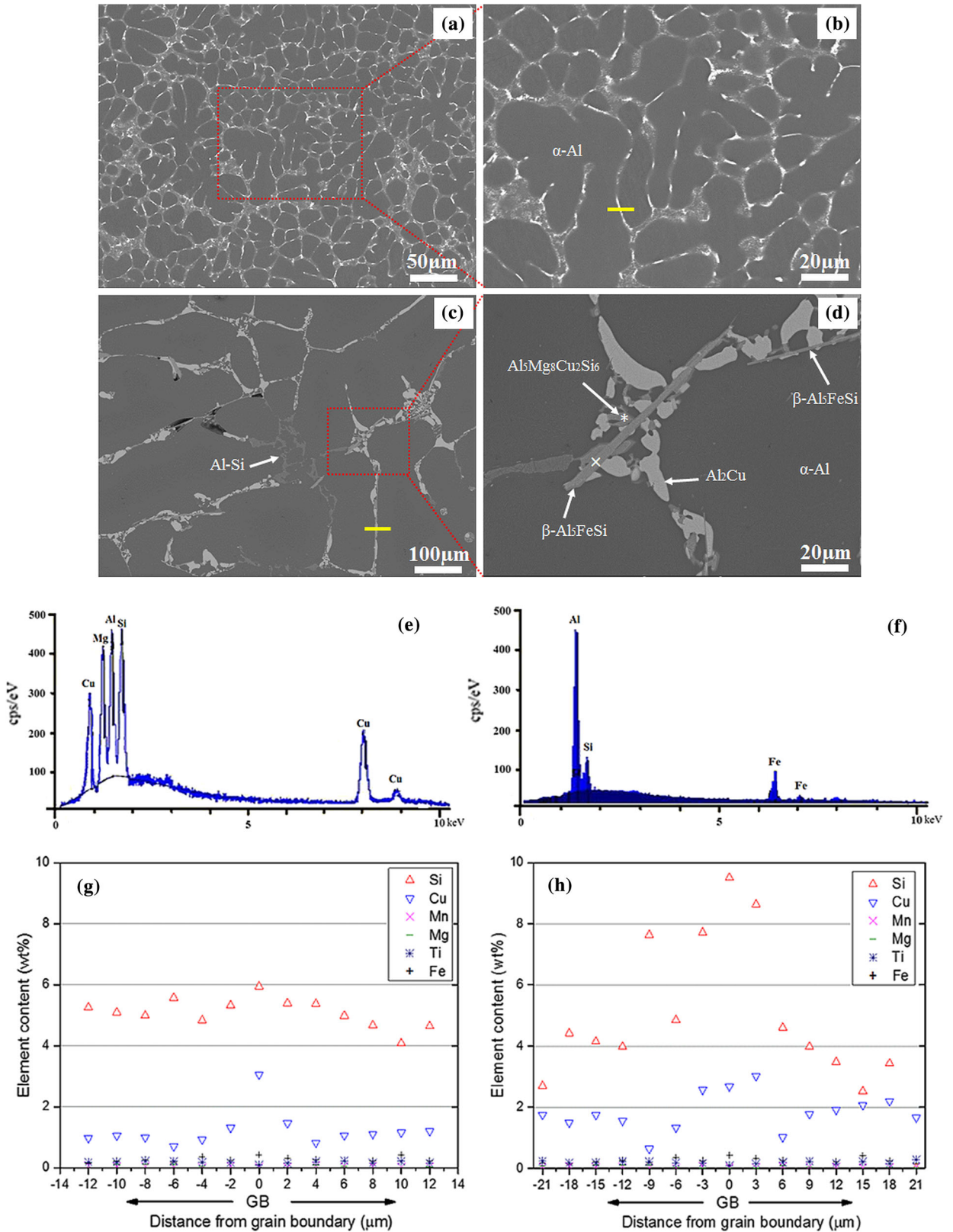


Fig. 5—Microstructures and EDX analysis of the 319s alloy: (a) as-received, (b) high-magnification micrograph showing grain boundaries, (c) after DSC test (d) high-magnification micrograph showing the intermetallic compounds, (e) EDX spectrum for $Al_5Mg_8Cu_2Si_6$, marked as asterisk in (d), (f) EDX spectrum for $\beta-Al_5FeSi$, marked as multiply symbol in (d), (g) line analysis across a grain boundary in (b), (h) line analysis across a grain boundary in (c).

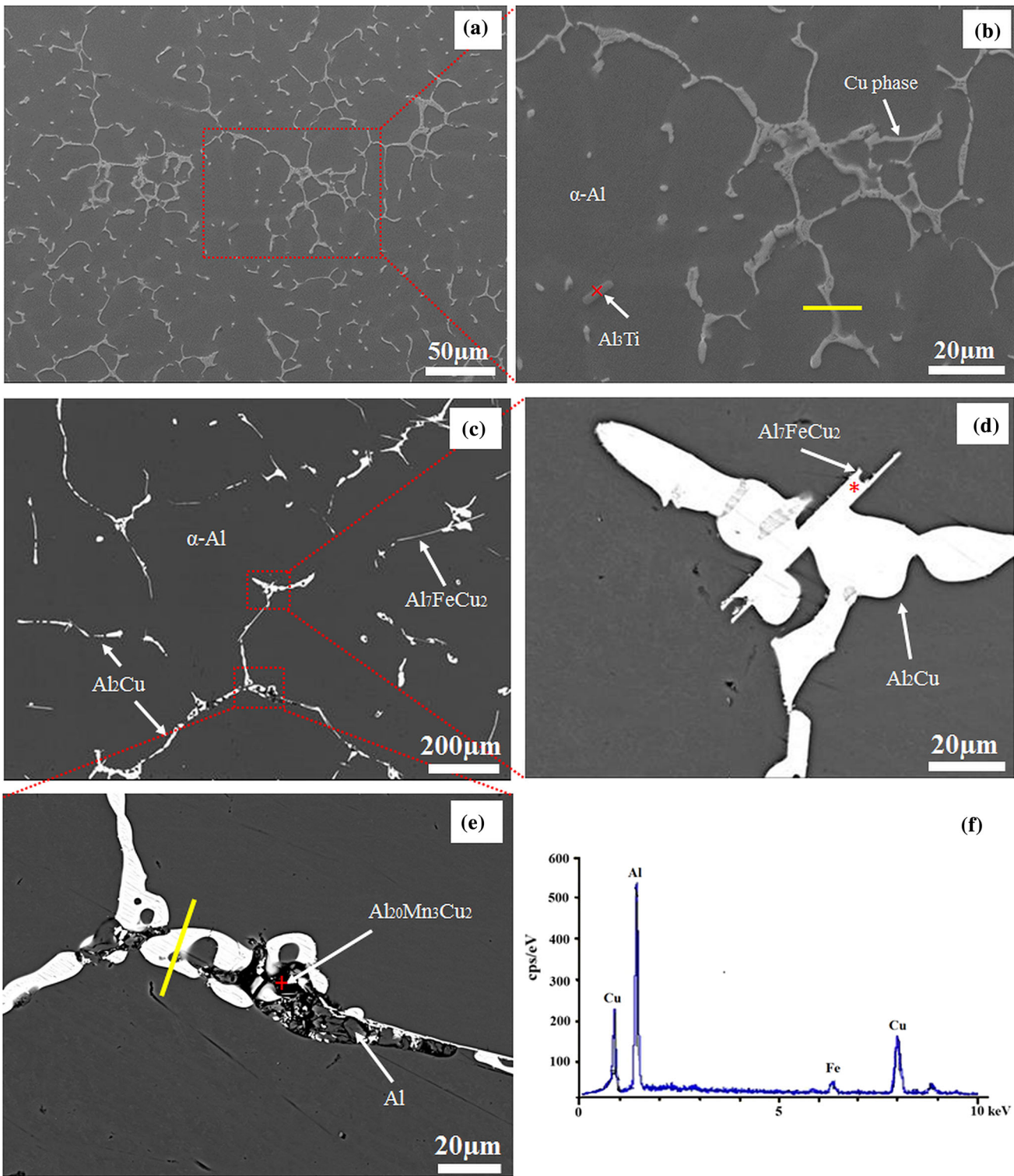


Fig. 6—Microstructures and EDX analysis of the 201 alloy: (a) as-received, (b) high-magnification micrograph showing grain boundaries and Al_3Ti particles, (c) after DSC test (d) high-magnification micrograph showing the Al_7FeCu_2 particle, (e) high-magnification micrograph showing the $\text{Al}_{20}\text{Mn}_3\text{Cu}_2$ particle, (f) EDX spectrum for Al_7FeCu_2 phase, marked as asterisk in (d), (g) EDX spectrum for $\text{Al}_{20}\text{Mn}_3\text{Cu}_2$ phase, marked as plus symbol in (e), (h) EDX spectrum for Al_3Ti phase, marked as multiply symbol in (b), (i) line analysis across a grain boundary in (b), (j) line analysis across a grain boundary in (e).

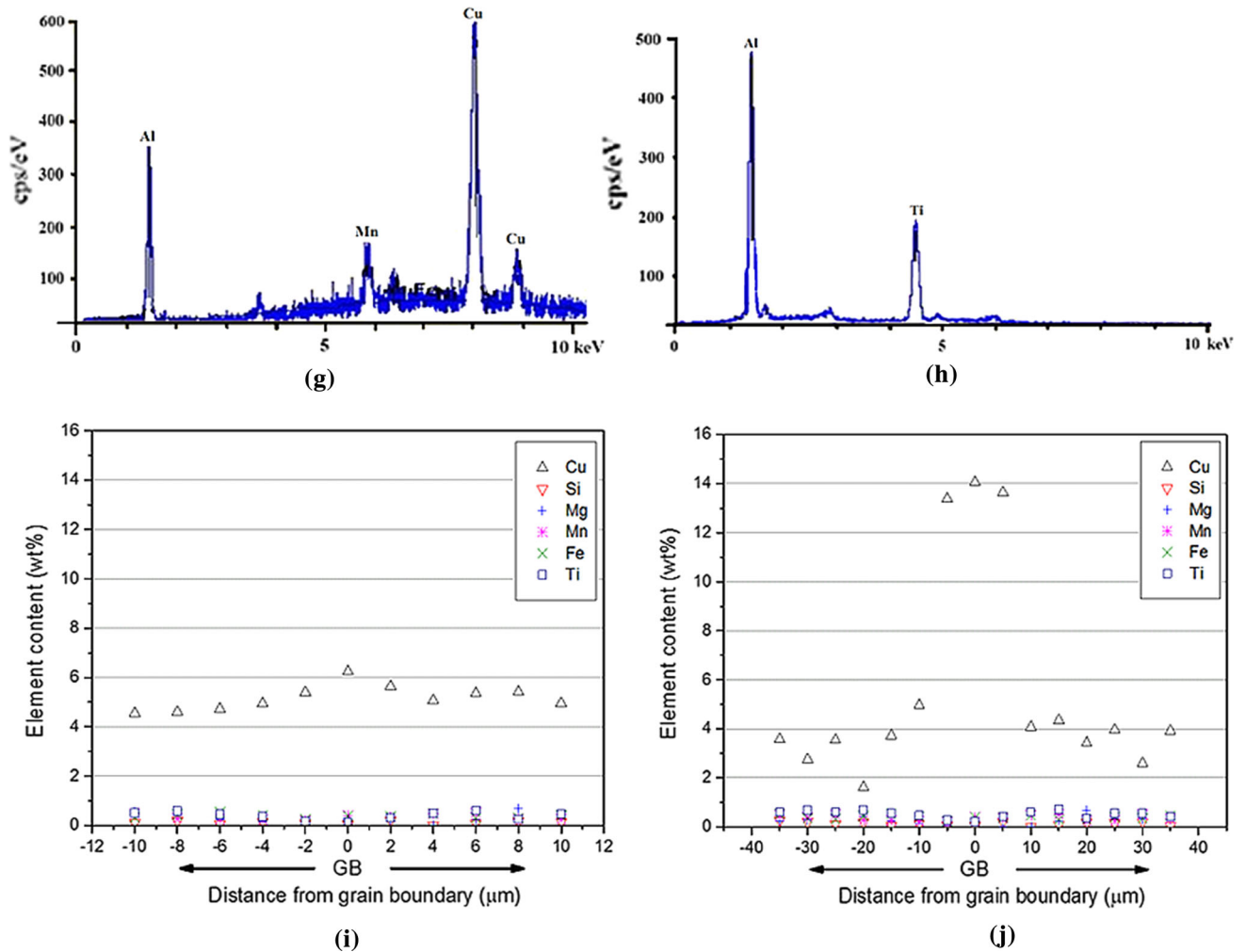


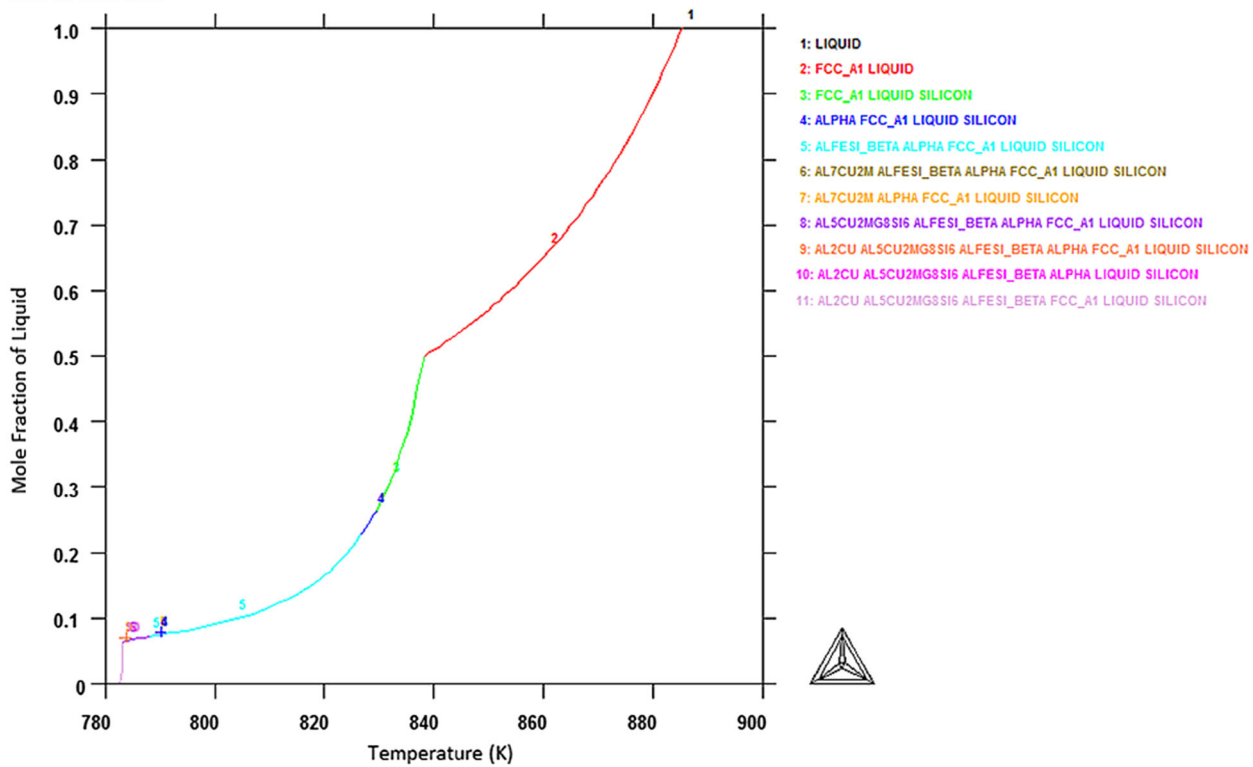
Fig. 6—continued.

that the Scheil model would not be appropriate for thermodynamic prediction of liquid fraction versus temperature for practical thixoforming with starting material which is MHD processed and that rather an equilibrium calculation should be used.

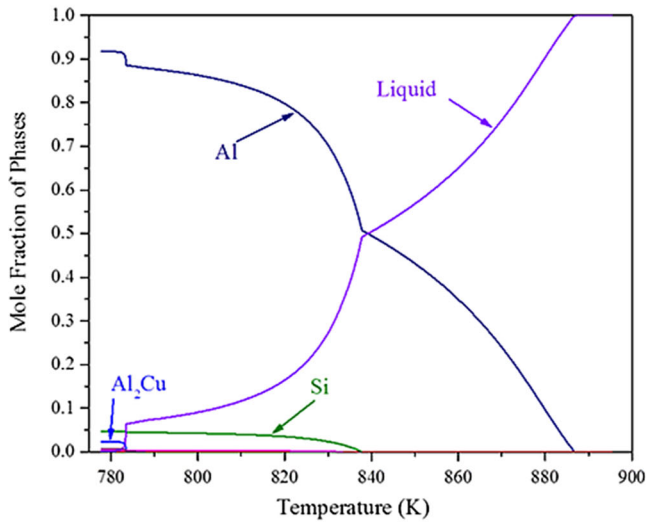
Figure 8 compares the liquid fraction-temperature relationships from Thermo-Calc for both Scheil and equilibrium assumptions with the results from DSC. The solidus for the equilibrium prediction is about 17 K higher than for the Scheil due to the effects of the microsegregation leading to incipient melting. With the Scheil prediction, there is an initial ‘knee’ whilst a ternary or quaternary reaction is occurring with the associated liquid formation. The liquid fraction is then higher for a given temperature than for the equilibrium prediction until a temperature of about 833 K (560 °C) where the two prediction curves coincide and are then almost superposed throughout the rest of the melting regime. Comparing then with the liquid fraction from the DSC for 1st heating and 2nd heating, the 1st heating is much more similar in shape to the equilibrium

prediction, with only one inflection point [the ‘knee’ at about 848 K (575 °C)]. The 2nd heating matches the Scheil prediction in shape with an initial ‘knee’ at about 788 K (515 °C) and then a further ‘knee’ at about 848 K (575 °C), coinciding with that on the 1st heating curve. The question is then why is the upper ‘knee’ displaced to a higher temperature for the DSC results in comparison with the predictions by about 10 K. Liu *et al.*^[10] discussed this and attributed it to kinetic factors but a detailed explanation is not clear.

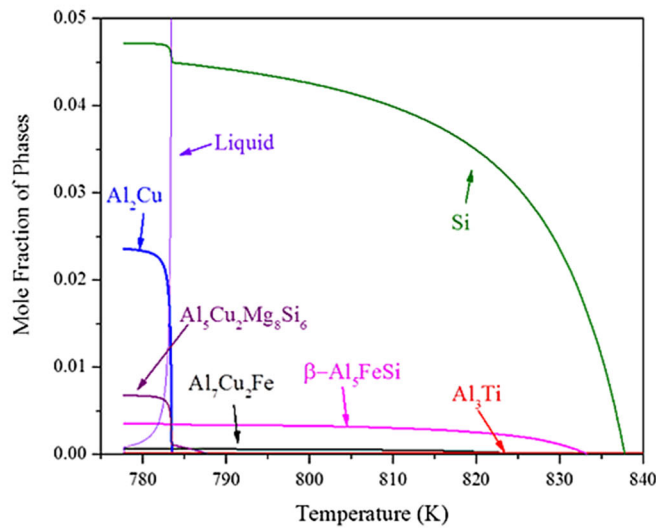
The cooling curve is identical for the 1st heating and the 2nd heating. The upper ‘knee’ is displaced to a lower temperature in comparison with both the prediction and the 1st and 2nd Heating curves. There is a lower ‘knee’, which again is displaced to a lower temperature. The distinction between the heating curve and the cooling curve is significant, and in the context of determining the processing window, it is the heating curve which should be used for thixoforming where the manufacturing method involves heating a billet from the solid state. If the DSC results were being used to predict the



(a)



(b)



(c)

Fig. 7—Thermo-Calc predicted phases (Scheil) for 319s alloy showing (a) liquid fraction vs temperature (b) Overall growth profile of all phases, (c) growth profile of minor secondary phases.

thixoforming processing temperature window they would indicate ~838 K to ~848 K (~565 °C to ~575 °C). If the thermodynamic predictions were used, the window would be ~833 K to ~838 K (~560 °C to ~565 °C). Although these distinctions in temperature

may not seem large, in practice they can be important in ensuring the process is repeatable and controllable so as to obtain a consistent product and to minimize ‘trial and error’ in establishing process parameters in industrial practice.

Table VIII. Temperatures (K) for Phase Reactions Calculated from Thermo-Calc for 319s Alloy (Scheil)

Reaction	Temperature [K (°C)]
1. (Al) Dendrite network	886 K (613 °C)
2. Precipitation of eutectic Si	837 K (564 °C)
3. Precipitation of β -AlFeSi	833 K (560 °C)
4. Precipitation of Al ₇ Cu ₂ Fe	827 K (554 °C)
5. Precipitation of Al ₅ Mg ₈ Cu ₂ Si ₆	788 K (515 °C)
6. Precipitation of Al ₂ Cu	783 K (510 °C)

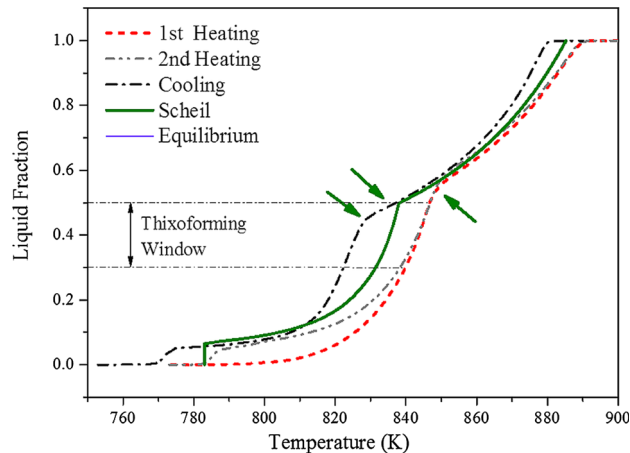


Fig. 8—Calculated liquid fraction vs temperature from DSC (3 K/min) for 319s alloy (~20 mg), together with Scheil and lever rule calculations. Arrows indicate the 'knees'.

IV. SUMMARY AND CONCLUSIONS

Two high-performance aluminum alloys of interest for commercial thixoforming (319s and 201) have been investigated with DSC and thermodynamic prediction software. The alloys were received in a state where they had been MHD stirred and then solidified. If reheated into the semisolid state, this would give the required microstructure for SSP of solid spheroids in a liquid matrix. In the DSC, the alloys have first been heated from the as-received state to fully liquid, then cooled, then re-heated and re-cooled. Comparing the two DSC curves, there are distinctions, with the second heat showing enhanced peaks, particularly for the initial stages of heating. The peaks have been compared with reactions identified in the literature. Combining the interpretation of the DSC results with microstructural observations supports the hypothesis that in the second heat, the alloys are in a strongly microsegregated state and it is this which is leading to the enhanced peaks for the minor phases which are generally complex intermetallics. The thermodynamic prediction results further reinforce this hypothesis.

The prediction of fraction liquid versus temperature is important for establishing the parameters for SSP. These results highlight that:

- (a) If DSC is to be used, the heating rate must be carefully chosen (given that it cannot match the rate of heating in the induction heating route typically used for thixoforming), as the DSC

- heating rate influences the fraction liquid versus temperature curve quite significantly;
- (b) With thermodynamic prediction, the equilibrium condition will provide better guidance for the thixoforming of MHD stirred starting material than the Scheil condition. The Scheil mode approximates more closely with a strongly microsegregated state.

ACKNOWLEDGMENTS

The authors would like to acknowledge the University of Leicester for financial support and support from the International Science and Technology Cooperation Projects of China (2012DFA50300) on material preparation. In addition, helpful conversations with Professor Veronique Favier at Arts et Metier ParisTech are gratefully acknowledged by HVA.

OPEN ACCESS

This article is distributed under the terms of the Creative Commons Attribution 4.0 International License (<http://creativecommons.org/licenses/by/4.0/>), which permits unrestricted use, distribution, and reproduction in any medium, provided you give appropriate credit to the original author(s) and the source, provide a link to the Creative Commons license, and indicate if changes were made.

REFERENCES

1. H.V. Atkinson: *Mater. Sci. Technol.*, 2010, vol. 26, pp. 1401–13.
2. I. Polmear: *Light alloys: from traditional alloys to nanocrystals*, 4th ed., Butterworth-Heinemann, Oxford, 2005, pp. 205–35.
3. G. Wallace, A.P. Jackson, S.P. Midson, and Q. Zhu: *Trans. Nonferrous Mater. Soc. China*, 2010, vol. 20, pp. 1786–91.
4. D. Liu, H.V. Atkinson, P. Kapranos, and H. Jones: *J. Mater. Sci.*, 2004, vol. 39, pp. 99–105.
5. L. Bäckerud, G. Chai, and J. Tamminen: *Solidification Characteristics of Aluminium Alloys: Foundry Alloys*, American Foundrymen's Society Inc, Schaumburg, 1990.
6. F.H. Samuel, A.M. Samuel, and H.W. Doty: *AFS Trans.*, 1996, vol. 104, pp. 893–901.
7. E.J. Martinez, M.A. Cisneros, S. Valtierra, and J. Lacaze: *Scripta Mater.*, 2005, vol. 52, pp. 439–43.
8. A.A. Kazakov: *Adv. Mater. Processes*, 2000, vol. 157, pp. 31–34.
9. Y.Q. Liu, A. Das, and Z. Fan: *Mater. Sci. Technol.*, 2004, vol. 20, pp. 35–41.
10. D. Liu, H.V. Atkinson, and H. Jones: *Acta Mater.*, 2005, vol. 53, pp. 3807–19.
11. L. Lasa and J.M. Rodriguez-Ibabe: *Mater. Charact.*, 2002, vol. 48, pp. 371–78.
12. F.H. Samuel: *J. Mater. Res.*, 1998, vol. 33, pp. 2283–97.
13. G. Wang, X. Bian, W. Wang, and J. Zhang: *Mater. Lett.*, 2003, vol. 57, pp. 4083–87.
14. Z. Li, A.M. Samuel, F.H. Samuel, C. Ravindran, and S. Valtierra: *J. Mater. Sci.*, 2003, vol. 38, pp. 1203–18.
15. S. Nafisi, D. Emadi, and R. Ghomashchi: *Mater. Sci. Eng.*, 2009, vol. 507, pp. 87–92.
16. Y. Birol: *J. Alloys Compd.*, 2009, vol. 486, pp. 173–77.
17. M.A.M. Arif, M.Z. Omar, N. Muhamad, J. Syarif, and P. Kapranos: *J. Mater. Sci.*, 2013, vol. 29, pp. 765–74.
18. G.L. Brollo, C.T.W. Proni, and L.C. de Paula: *Thermochimica Acta*, 2017, vol. 651, pp. 22–33.

19. D. Zhang, H.V. Atkinson, H.B. Dong, and Q. Zhu: *Solid State Phenom.*, 2015, vols. 217–218, pp. 442–49.
20. G. Gottardi, A. Pola, and G.M. La Vecchia: *La Metallurgia Italiana*, 2015, vol. 5, pp. 11–16.
21. A. Lombardi, A. Elsayed, D. Sediako, and C. Ravindran: *J. Alloys Compd.*, 2017, vol. 695, pp. 2628–36.
22. J.G. Kaufman and E.L. Rooy: *Aluminum Alloy Castings: Properties, Processes, and Applications*, ASM International, Ohio, 2004.
23. D. Larouche, C. Laroche, and M. Bouchard: *Acta Mater.*, 2003, vol. 51, pp. 2161–70.
24. H.B. Dong, M.R.M. Shin, E.C. Kurum, H. Cama, and J.D. Hunt: *Fluid Phase Equilib.*, 2003, vol. 212, pp. 199–208.
25. Information on <http://www.thermocalc.com/products-services/databases/thermodynamic>.
26. M.C. Flemings: *Metall. Trans.*, 1974, vol. 5, pp. 2121–34.
27. A. Samuel, J. Gauthier, and F. Samuel: *Metall. Mater. Trans. A*, 1996, vol. 27A, pp. 1785–98.
28. G. Höhne, W.F. Hemminger, and H.J. Flammersheim: *Differential Scanning Calorimetry*, 2nd ed., Springer, New York, 2003.